Residence times and other functionals of reflected Brownian motion

D. S. Grebenkov*
Laboratoire de Physique de la Matière Condensée, CNRS–Ecole Polytechnique, 91128 Palaiseau, France
(Received 4 April 2007; published 30 October 2007)

We study the residence and local times for a Brownian particle confined by reflecting boundaries, and propose a general solution to the problem of finding the related probability distribution. Its Fourier transform (characteristic function) and Laplace transform (survival probability) are obtained in a compact matrix form involving the Laplace operator eigenbasis. Explicit combinatorial relations are derived for the moments, and the probability distribution is shown to be nearly Gaussian when the exploration time is long enough. When the eigenbasis (or a part of it) is known, the numerical computation of the residence time distributions is straightforward and accurate. The present approach can also be applied to investigate other functionals of reflected Brownian motion describing, in particular, restricted diffusion in an external field or potential (e.g., nuclei diffusing in an inhomogeneous magnetic field). Theoretical results for the local times are confronted with Monte Carlo simulations on the unit interval, disk, and sphere.

DOI: 10.1103/PhysRevE.76.041139 PACS number(s): 05.40.Jc, 02.50.−r, 05.10.−a, 05.60.−k

I. INTRODUCTION

Diffusion is a fundamental transport mechanism for many physical, chemical, biological, and industrial systems [1,2]. In the course of its motion, each diffusing species explores different regions of the bulk. Since reactive zones are often heterogeneously distributed in the bulk (e.g., in a chemical reactor or biological cell), the net outcome and the whole functioning of the system strongly depend on how long the diffusing species remains in these zones. These so-called residence or occupation times are relevant for various diffusion-influenced reactions, e.g., energy transfer [3,4] or fluorescence quenching [5]. In optical imaging of turbid media, longer diffusive photon migration can indicate abnormal regions in the tissue such as tumors [6]. The residence times have thus been thoroughly studied for different stochastic processes [7–19].

In most cases, however, the motion of diffusing species is restricted by a geometrical confinement, resulting in drastic modifications of the transport. The microscopic interaction between the species and the surface depends on their physicochemical or biological properties. For instance, paramagnetic impurities dispersed on the boundary cause surface relaxation in nuclear magnetic resonance (NMR) experiments [20,21]; catalytic seeds distributed over the boundary initiate chemical transformation of the diffusing species [22–24]; permeability of the alveolar membranes allows oxygen transfer to the blood [25,26]. A realistic description of these processes at the microscopic level is a challenging problem, demanding, for example, accurate molecular dynamics simulations near the interface, or quantum mechanics calculations. At the time scale of the macroscopic transport process, however, the contact with the interface is very rapid so that the precise description of the interaction may be irrelevant (if there is no anomalously long-time trapping or localization on the interface).[1] In most cases, interactions yield one of two opposite events: a species changes its state (loss of magnetization, absorption, transfer, or chemical transformation) and no longer participates in transport; or, after a short adsorption, interaction, or waiting time τ, the diffusive motion is resumed from an ε vicinity of the hitting point and continued in the bulk, until the next contact with the interface, and so on.

In other words, the species interacts with the boundary in its neighboring ε layer which is treated as a "black box:" after a short time τ, the species is somehow "released" at a distance of the order of ε. In this coarse-grained picture, the specific nature of the interaction determines the values (or the probability distributions) of the adsorption time τ and the layer width ε. What really matters here is that the species leaves the interface and continues its diffusive motion.

The whole trajectory in a bounded domain is then often modeled either by lattice random walks [27,28] or as a sequence of Brownian flights [29–32]. In the former case, the interaction parameters ε and τ determine the discretization mesh and hopping rate, respectively [Fig. 1(a)]. Although lattice random walks can be very easily implemented for various domains, the numerical computation becomes inefficient in many practical situations when the microscopic parameters ε and τ are too small as compared to macroscopic transport scales. In turn, Brownian flights are composed of continuous Brownian trajectories which are interrupted by discontinuous jumps in the vicinity of the interface [Fig. 1(b)]. In this case, efficient analytical tools can be applied to investigate each Brownian flight, while the analysis of the whole trajectory is still difficult, since the statistics of jumps strongly depends on Brownian flights, and vice versa.

In this paper, we follow another strategy by modeling the whole trajectory, even in close vicinity to the interface, as a

*denis.grebenkov@polytechnique.edu

[1] At the same time, it is worth noting that certain interactions may lead to trapping or long-time localization of the species on the boundary. During this adsorption state, the species can travel long distances along this boundary as in the case of some proteins attaching to DNA and searching for its specific regions. We do not consider such cases in this paper.

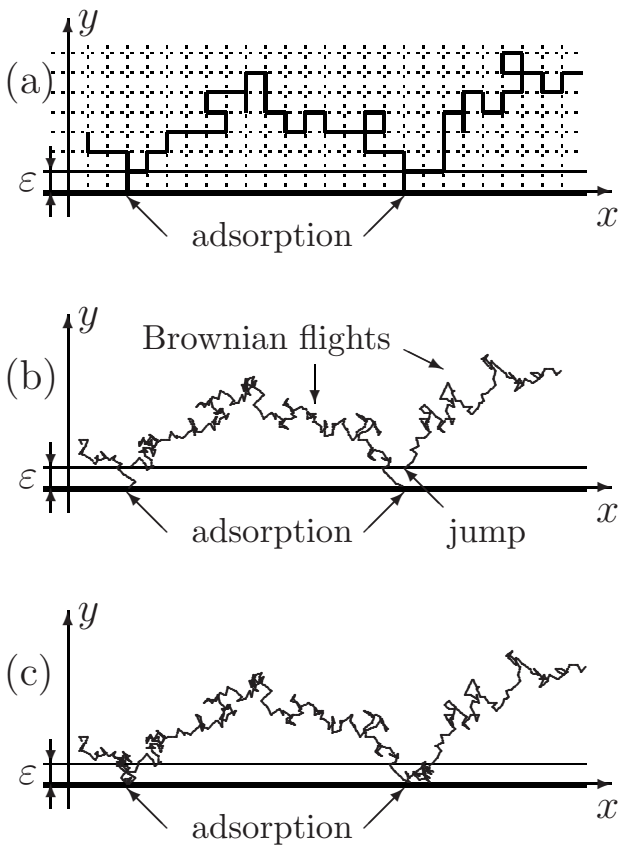

FIG. 1. Three "strategies" for modeling the trajectory of the diffusing species with interactions in the ε vicinity of the interface (horizontal axis): (a) discrete random walks with step ε, (b) Brownian flights with jumps at distance ε, and (c) the reflected Brownian motion. In all three cases, the interaction is considered as a kind of reflection event.

continuous path of *reflected Brownian motion* [Fig. 1(c)]. The simplest example of this process is the modulus of a one-dimensional Brownian motion x_t: $X_t=|x_t|$. Each time a diffusing species crosses the boundary (end point 0), it is reflected toward the bulk (positive semi-infinite interval). In general, reflected Brownian motion is constructed as a solution of the stochastic differential equation accounting for reflections on the boundary of the confining domain [33].

In sharp contrast with ordinary Brownian motion, the construction of reflected Brownian motion strongly depends on the geometry of the confining medium, being especially sophisticated for irregular boundaries. From this point of view, this strategy may sound like a complication of the interaction event, when a simple linear jump is replaced by a trace of a complex stochastic process. Moreover, the behavior of this process in the vicinity of the interface may seem contradictory to physical intuition. For example, the number of reflections during an infinitesimal time after the first contact with the interface is infinite. It is important to stress, however, that these mathematical "paradoxes" emerge only in the limit of very short length scales, much smaller than the interaction layer width ε. Similarly, the ordinary Brownian motion can reasonably model molecular dynamics only *above* a certain length scale. Once a physical cutoff ε is fixed, the adsorption time τ appears as the first exit time of the reflected Brownian motion from the ε vicinity of the boundary. Alternatively, one can fix τ and consider the width ε to be spread, providing another way to adjust the present coarse-grained modeling to realistic interactions with the boundary. Note also that reflected Brownian motion is implicitly employed whenever a diffusion equation with Neumann boundary condition is involved. Consequently, the reflected Brownian motion is in fact a natural tool for modeling diffusive motion in confined media.

What we gain by considering reflected Brownian motion is that the whole dynamics can be treated in a single mathematical frame. In this paper, we illustrate this advantage for investigation of the residence times and other functionals of this stochastic process.

II. EIGENMODE EXPANSION

For a given function $B(\mathbf{r})$ in a bounded domain Ω with a smooth boundary $\partial\Omega$,[2] we consider the random variable

$$\phi = \int_0^t ds\, B(X_s), \tag{1}$$

X_s being a random trajectory of the reflected Brownian motion in Ω, starting with a given initial density $\rho(\mathbf{r}_0)$.[3] Intuitively, the function $B(\mathbf{r})$ can be thought of as a distribution of "markers" to distinguish different points or regions of the confining domain. When the diffusing species passes through these regions, the random variable ϕ accumulates the corresponding marks. In other words, different parts of the trajectory are weighted according to the function $B(\mathbf{r})$, encoding thus the whole stochastic process. For example, if the bulk contains absorbing sinks or relaxing impurities, $B(\mathbf{r})$ can represent the distribution of their absorption or relaxation rates. Here ϕ is the cumulant absorption factor penalizing the trajectories that pass through the sinks. In NMR, the encoding mechanism is experimentally realized by applying an inhomogeneous magnetic field $B(\mathbf{r})$ (typically with a linear gradient over the sample Ω). In this case, ϕ is the total phase accumulated by an individual spin-bearing particle during its restricted diffusion in this field [34].

A. Probability distribution

The probability distribution of the random variable ϕ will be found in two steps. The first step is based on the classical Kac result [7–9] relating the expectation $\mathbb{E}\{e^{-h\phi}\}$ to the solution of a diffusion equation with bulk relaxation. This expectation includes the average of the functional $e^{-h\phi}$ over all random trajectories $\{X_s\}_{0\le s\le t}$ of the reflected Brownian motion between the starting point $\mathbf{r}_0$ at time 0 and the arrival at

[2]The boundary $\partial\Omega$ of the confining domain Ω is assumed to be smooth (twice continuously differentiable). This purely mathematical assumption, irrelevant for most physical problems, can be considerably weakened.

[3]In general, $B(\mathbf{r})$ can be weighted by an effective temporal profile (see Refs. [34,45] for more details).

point $\mathbf{r}$ at time t, as well as the average over all $\mathbf{r}_0$ and $\mathbf{r}$ with a given initial density $\rho(\mathbf{r}_0)$ and weight (or pickup) function $\tilde{\rho}(\mathbf{r})$, respectively. In this case, Kac's result reads as

$$\mathbb{E}\{e^{-h\phi}\} = \int_\Omega d\mathbf{r}\ \mathfrak{m}(\mathbf{r},t)\tilde{\rho}(\mathbf{r}), \tag{2}$$

where $\mathfrak{m}(\mathbf{r},t)$ obeys the equation

$$\frac{\partial \mathfrak{m}(\mathbf{r},t)}{\partial t} - \Delta \mathfrak{m}(\mathbf{r},t) + hB(\mathbf{r})\mathfrak{m}(\mathbf{r},t) = 0, \tag{3}$$

with the initial condition $\mathfrak{m}(\mathbf{r}_0,t=0)=\rho(\mathbf{r}_0)$, and $\Delta = \partial^2/\partial x_1^2 + \cdots + \partial^2/\partial x_d^2$ is the Laplace operator in d dimensions. The reflecting character of Brownian motion is represented by Neumann boundary conditions, when the normal derivative at the boundary vanishes: $\partial \mathfrak{m}(\mathbf{r},t)/\partial n = 0$ on $\partial\Omega$. Note that the diffusion coefficient (fixed to be 1 here) can be introduced by rescaling the time variable. If $B(\mathbf{r})$ is the distribution of bulk sinks (or their absorption rates), $\mathfrak{m}(\mathbf{r},t)$ can be interpreted as the probability density for a Brownian particle, starting with the initial density $\rho(\mathbf{r}_0)$, to arrive in an infinitesimal vicinity of the point $\mathbf{r}$ at time t, without being absorbed during its motion. The weight function $\tilde{\rho}(\mathbf{r})$ allows one to delimit the region of interest in the whole confining domain. Since $\mathfrak{m}(\mathbf{r},t)$ is weighted by $\tilde{\rho}(\mathbf{r})$ in Eq. (2), only those Brownian trajectories that arrived into pickup regions at time t can contribute to the expectation of ϕ.

At the second step, the solution $\mathfrak{m}(\mathbf{r},t)$ is expanded over the complete orthonormal basis of the Laplace operator eigenfunctions $u_m(\mathbf{r})$:

$$\mathfrak{m}(\mathbf{r},t) = \sum_{m'} c_{m'}(t) u_{m'}(\mathbf{r}). \tag{4}$$

Substitution of this expansion in Eq. (3), multiplication by $u_m^*(\mathbf{r})$, and integration over Ω yield a set of ordinary differential equations for the unknown coefficients $c_m(t)$,

$$\frac{\partial c_m(t)}{\partial t} + \sum_{m'} (\Lambda_{m,m'} + h\mathcal{B}_{m,m'}) c_{m'}(t) = 0, \tag{5}$$

where the infinite-dimensional matrices $\mathcal{B}$ and Λ are

$$\mathcal{B}_{m,m'} = \int_\Omega d\mathbf{r}\ u_m^*(\mathbf{r}) B(\mathbf{r}) u_{m'}(\mathbf{r}), \tag{6}$$

$$\Lambda_{m,m'} = \delta_{m,m'}\lambda_m, \tag{7}$$

λ_m being the Laplace operator eigenvalues. Thinking of $c_m(t)$ as components of an infinite-dimensional vector $C(t)$, one easily finds the solution of the above matrix equation. The expectation $\mathbb{E}\{e^{-h\phi}\}$ can thus be written in the compact matrix form of a scalar product:

$$\mathbb{E}\{e^{-h\phi}\} = (U\ \ e^{-(h\mathcal{B}+\Lambda)t}\ \ \tilde{U}), \tag{8}$$

where the infinite-dimensional vectors U and $\tilde{U}$ represent the projections of the initial density $\rho(\mathbf{r})$ and of the weight function $\tilde{\rho}(\mathbf{r})$ onto the eigenfunctions $u_m(\mathbf{r})$:

$$U_m = V^{1/2} \int_\Omega d\mathbf{r}\ u_m^*(\mathbf{r})\rho(\mathbf{r}), \tag{9}$$

$$\tilde{U}_m = V^{-1/2} \int_\Omega d\mathbf{r}\ u_m(\mathbf{r})\tilde{\rho}(\mathbf{r}), \tag{10}$$

V being the volume of the domain. From a quantum-mechanical point of view, the matrices Λ and $\mathcal{B}$ correspond to a free Hamiltonian and a perturbing interaction, respectively. The matrix $e^{-(h\mathcal{B}+\Lambda)t}$ can thus be thought of as a kind of evolution operator acting on the initial state $\rho(\mathbf{r})$ (represented by vector U). The resulting density $\mathfrak{m}(\mathbf{r},t)$ at time t is then weighted by the pickup function $\tilde{\rho}(\mathbf{r})$ (represented by the vector $\tilde{U}$). It is important to note that the matrices $\mathcal{B}$ and Λ do not commute.

The closed matrix form (8) is one of the central relations in this paper. It provides a complete probabilistic description of the random variable ϕ. For positive h, the expectation $\mathbb{E}\{e^{-h\phi}\}$ can be interpreted as the Laplace transform of the probability distribution of ϕ, allowing one to find the latter by inverse Laplace transform.

The formal substitution of $h=-iq$ into Eq. (8) gives the characteristic function of ϕ:

$$\mathbb{E}\{e^{iq\phi}\} = (U\ \ e^{(iq\mathcal{B}-\Lambda)t}\ \ \tilde{U}). \tag{11}$$

Its inverse Fourier transform yields again the probability distribution of ϕ, while the series expansion of $e^{iq\phi}$ generates all its moments:

$$\mathbb{E}\{e^{iq\phi}\} = \sum_{n=0}^{\infty} \frac{(iq)^n}{n!} \mathbb{E}\{\phi^n\}. \tag{12}$$

B. Moments

The moments of the random variable ϕ can also be written according to their probabilistic definition (see [34] for more details). For instance, the first moment is

$$\mathbb{E}\{\phi\} = \int_0^t dt_1 \int_\Omega d\mathbf{r}_0 \int_\Omega d\mathbf{r}_1 \int_\Omega d\mathbf{r}_2\ \ \rho(\mathbf{r}_0) \times G_{t_1}(\mathbf{r}_0,\mathbf{r}_1) B(\mathbf{r}_1) G_{t-t_1}(\mathbf{r}_1,\mathbf{r}_2)\tilde{\rho}(\mathbf{r}_2),$$

where $G_t(\mathbf{r},\mathbf{r}')$ is known as the diffusive propagator, heat kernel, or, equivalently, Green function of the diffusion equation. This equation has a simple probabilistic interpretation. In fact, the random variable ϕ depends on the whole Brownian trajectory by its definition (1). The contribution $B(\mathbf{r}_1)$ to this variable at time t_1 is obtained by averaging over all Brownian trajectories passing through the point $\mathbf{r}_1 = X_{t_1}$. In other words, we consider all random walkers starting at $\mathbf{r}_0$ [with probability $\rho(\mathbf{r}_0)d\mathbf{r}_0$], diffusing until time t_1 into the vicinity of $\mathbf{r}_1$ [with probability $G_{t_1}(\mathbf{r}_0,\mathbf{r}_1)d\mathbf{r}_1$], and diffusing until time t into the vicinity of $\mathbf{r}_2$ [with probability $G_{t-t_1}(\mathbf{r}_1,\mathbf{r}_2)d\mathbf{r}_2$], which should be "allowed" by the pickup function $\tilde{\rho}(\mathbf{r}_2)$. Using the eigenmode expansion for the heat kernel,

$$G_t(\mathbf{r},\mathbf{r}') = \sum_{m=0}^{\infty} u_m^*(\mathbf{r}) u_m(\mathbf{r}') e^{-t\lambda_m},$$

one gets another expression for the first moment,

$$\mathbb{E}\{\phi\} = \int_0^t dt_1 \sum_{m_1=0}^{\infty} \sum_{m_2=0}^{\infty} U_{m_1} e^{-\lambda_{m_1} t_1} \mathcal{B}_{m_1,m_2} e^{-\lambda_{m_2}(t-t_1)} \tilde{U}_{m_2}.$$

Representing the eigenvalues λ_m by the diagonal matrix Λ, one can write the above relation in a compact form,

$$\mathbb{E}\{\phi\} = \int_0^t dt_1 (U e^{-\Lambda t_1} \mathcal{B} e^{-\Lambda(t-t_1)} \tilde{U}). \tag{13}$$

Here, U, $e^{-\Lambda t}$, $\mathcal{B}$, and $\tilde{U}$ are the matrix representations in the Laplace operator eigenbasis for $\rho(\mathbf{r})$, $G_t(\mathbf{r},\mathbf{r}')$, $B(\mathbf{r})$, and $\tilde{\rho}(\mathbf{r})$, respectively. Surprisingly, this expression appears to be more cumbersome than Eq. (11) for the characteristic function. It is worth noting that the diffusion equation (3) with an imaginary last term was considered by Torrey to describe the transverse magnetization evolution in NMR [35]. In that case, the function $B(\mathbf{r})$ might also be time dependent. A similar matrix formalism has recently been developed in this field [34,36–39].

Higher-order moments can also be written in a compact matrix form [34]:

$$\mathbb{E}\{\phi^n\} = n! \int_0^t dt_1 \int_{t_1}^t dt_2 \cdots \int_{t_{n-1}}^t dt_n (U e^{-\Lambda t_1} \mathcal{B} e^{-\Lambda(t_2-t_1)} \times \mathcal{B} \cdots \mathcal{B} e^{-\Lambda(t_n-t_{n-1})} \mathcal{B} e^{-\Lambda(t-t_n)} \tilde{U}) \tag{14}$$

or, with explicit matrix summations,

$$\mathbb{E}\{\phi^n\} = n! \sum_{m_1=0}^{\infty} \cdots \sum_{m_{n+1}=0}^{\infty} U_{m_1} \mathcal{B}_{m_1,m_2} \mathcal{B}_{m_2,m_3} \cdots \mathcal{B}_{m_n,m_{n+1}} \tilde{U}_{m_{n+1}} \times F_n(t;\lambda_{m_1},\ldots,\lambda_{m_{n+1}}), \tag{15}$$

where

$$F_n(t;\lambda_{m_1},\ldots,\lambda_{m_{n+1}}) \equiv \int_0^t dt_1 \int_{t_1}^t dt_2 \cdots \int_{t_{n-1}}^t dt_n \times e^{-\lambda_{m_1} t_1} e^{-\lambda_{m_2}(t_2-t_1)} \cdots e^{-\lambda_{m_{n+1}}(t-t_n)}.$$

These time integrals can be computed explicitly:

$$F_n(t;\lambda_{m_1},\ldots,\lambda_{m_{n+1}}) = (-1)^n \sum_{k=1}^{n+1} e^{-t\lambda_{m_k}} \prod_{\substack{j=1 \\ j\neq k}}^{n+1} \frac{1}{\lambda_{m_k} - \lambda_{m_j}}. \tag{16}$$

Although Eqs. (15) and (16) are exact and can in principle be used to calculate the moments, general analysis is still difficult.

C. Long-time behavior

A considerable simplification comes at long enough time t so that $t\lambda_1 \gg 1$, where λ_1 is the first nonzero eigenvalue (we recall that $\lambda_0 = 0$ for the Neumann boundary conditions considered here). In this case, all terms containing factors $e^{-t\lambda_{m_k}}$ with $m_k > 0$ are exponentially small and can thus be neglected. The only nontrivial contributions come from the terms for which some indices m_k are zero. For instance, direct computation shows that

$$F_n(t;\underbrace{0,0,\ldots,0}_{n+1}) = \frac{t^n}{n!}. \tag{17}$$

When k indices $m_{i_1}, m_{i_2}, \ldots, m_{i_k}$ are nonzero (here $i_1,\ldots,i_k$ denote arbitrary positions of nonzero entries, taking distinct values between 1 and $n+1$), one finds

$$F_n(t;\underbrace{0,\ldots,0}_{i_1-1},\lambda_{m_{i_1}},0,\ldots,\ldots,0,\lambda_{m_{i_k}},\underbrace{0,\ldots,0}_{n+1-i_k}) \simeq \sum_{\ell=0}^{n-k} (-1)^\ell \frac{t^{n-k-\ell}}{(n-k-\ell)!} \sum_{\substack{0\le j_i\le \ell (1\le i\le k), \\ j_1+\cdots+j_k=(k-1)\ell}} \lambda_{m_{i_1}}^{j_1-\ell-1} \cdots \lambda_{m_{i_k}}^{j_k-\ell-1} \tag{18}$$

(see Appendices for more details and some examples). The corrections to this relation are exponentially small and will be neglected in the remainder of the paper. Consequently, the moment $\mathbb{E}\{\phi^n\}$ as a function of time t turns out to be a polynomial of degree n at long time t:

$$\mathbb{E}\{\phi^n\} \simeq \sum_{k=0}^{n} a_{n,k}\ t^k. \tag{19}$$

According to Eq. (17), the coefficient in front of the highest-degree term t^n can be calculated by setting all indices $m_1,\ldots,m_{n+1}$ to 0 in Eq. (15):

$$a_{n,n} = n!\, U_0 \underbrace{\mathcal{B}_{0,0}\mathcal{B}_{0,0}\cdots\mathcal{B}_{0,0}}_{n \text{ times}} \tilde{U}_0 F_n(t;\underbrace{0,\ldots,0}_{n+1}) = t^n (\mathcal{B}_{0,0})^n. \tag{20}$$

Here we employed the fact that $U_0 = \tilde{U}_0 = 1$ for any initial density $\rho(\mathbf{r})$ and weight function $\tilde{\rho}(\mathbf{r})$, since the lowest eigenmode of the Laplace operator with Neumann boundary conditions is a constant function: $u_0(\mathbf{r}) = V^{-1/2}$. The coefficients in front of lower-degree terms are determined by other choices of the indices $m_1,\ldots,m_{n+1}$. As shown in Appendices, Eqs. (15) and (18) lead to explicit relations for the moments. However, even for $n=4$, the formulas are very lengthy, containing a large number of terms.

Remarkably, the combinatorial analysis can be significantly simplified by considering *cumulant moments* generated by a series expansion of the logarithm of the characteristic function:

$$\ln \mathbb{E}\{e^{iq\phi}\} \equiv \sum_{n=1}^{\infty} \frac{(iq)^n}{n!} < \phi^n > . \tag{21}$$

By substituting the series expansion (12) into the left-hand side of the above relation and reexpanding the logarithm in a power series, one can express the cumulant moments through the ordinary moments, e.g.,

$$<\phi> = \mathbb{E}\{\phi\},$$

$$<\phi^2> = \mathbb{E}\{\phi^2\} - (\mathbb{E}\{\phi\})^2,$$

$$<\phi^3> = \mathbb{E}\{\phi^3\} - 3\mathbb{E}\{\phi^2\}\mathbb{E}\{\phi\} + 2(\mathbb{E}\{\phi\})^3,$$

$$<\phi^4> = \mathbb{E}\{\phi^4\} - 4\mathbb{E}\{\phi^3\}\mathbb{E}\{\phi\} - 3(\mathbb{E}\{\phi^2\})^2 + 12\mathbb{E}\{\phi^2\}(\mathbb{E}\{\phi\})^2 - 6(\mathbb{E}\{\phi\})^4. \quad (22)$$

In general, the following recursion formula holds [40]:

$$<\phi^n> = \mathbb{E}\{\phi^n\} - \sum_{k=1}^{n-1} C_{n-1}^{k-1} <\phi^k> \mathbb{E}\{\phi^{n-k}\}, \quad (23)$$

C_n^k being the binomial coefficients. The cumulant moments are particularly useful when a random variable is close to being Gaussian. In fact, the characteristic function of a normally distributed random variable is Gaussian, so that the power series expansion of its logarithm is simply a square polynomial, i.e., all cumulant moments with $n>2$ are strictly zero. When the random variable is not Gaussian, the cumulant moments may quantify its deviation from Gaussian.

In Appendices, we argue that all cumulant moments are first-order polynomials of time t:

$$<\phi^n> \simeq b_{n,1}t + b_{n,0} \quad (24)$$

(up to exponentially small corrections). This statement is demonstrated for the cumulant moments up to $n=4$ and numerically checked for some higher moments. Its rigorous proof requires a substantial combinatorial analysis and is beyond the scope of this paper. Moreover, we give explicit formulas for the coefficients $b_{n,1}$ and $b_{n,0}$ in terms of the matrices $\mathcal{B}$ and Λ and vectors U and $\tilde{U}$ (see Appendices). The expressions for the moments $\mathbb{E}\{\phi^n\}$ can be deduced using the above relations.

At this moment, several qualitative conclusions can be made. Except for some trivial choices of the function $B(\mathbf{r})$, the random variable ϕ is not Gaussian since higher-order cumulant moments are not zero. Since the variance $<\phi^2>$ linearly increase in time, it is natural to renormalize ϕ by $\sqrt{t}$. The first cumulant moment of the new random variable $\phi/\sqrt{t}$ is still increasing in time, while its variance approaches a constant. In contrast, higher-order cumulant moments with $n>2$ go to 0. In the limit of very long time, the probability distribution of the normalized random variable $\phi/\sqrt{t}$ becomes closer and closer to a Gaussian distribution with mean $b_{1,1}\sqrt{t}$ and variance $b_{2,1}$, where

$$b_{1,1} = \mathcal{B}_{0,0}, \quad b_{2,1} = 2\sum_{m=1}^{\infty} \mathcal{B}_{0,m}\lambda_m^{-1}\mathcal{B}_{0,m} \quad (25)$$

(see Appendices). As a consequence, the probability distribution of ϕ at long time t is close to

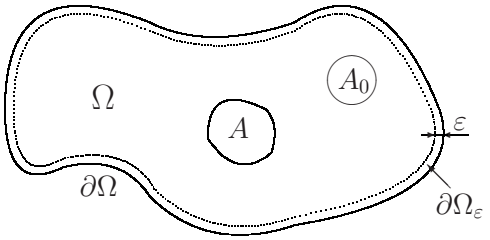

FIG. 2. Diffusive motion of species restricted inside a bounded confining domain Ω with reflecting boundary $\partial\Omega$. The residence time ϕ indicates how long a diffusing species, starting somewhere in the domain (e.g., in the subset A_0), spends in a subset A until time t. The local time shows how long the species spends in a close neighborhood (ε vicinity or ε sausage $\partial\Omega_\varepsilon$) of the boundary $\partial\Omega$.

$$\mathbb{P}\{\phi \in (x, x+dx)\} \simeq \frac{dx}{(2\pi b_{2,1}t)^{1/2}} \exp\left(-\frac{(x-b_{1,1}t)^2}{2b_{2,1}t}\right). \quad (26)$$

In the course of exploration, the mean value and the variance increase linearly, spreading the Gaussian distribution and shifting it to the right (Fig. 4).

D. Residence times

In the remainder of this paper, the matrix formalism will be applied to investigate the residence times of reflected Brownian motion. Let A be a subset of the confining domain Ω (Fig. 2). How long does the diffusing species reside on this subset? The characteristic function of this residence time is given by Eq. (11) with the matrix $\mathcal{B}$ determined by substituting $B(\mathbf{r}) = \mathbb{I}_A(\mathbf{r})$ in Eq. (6):

$$\mathcal{B}_{m,m'} = \int_A d\mathbf{r}\, u_m^*(\mathbf{r}) u_{m'}(\mathbf{r}), \quad (27)$$

where $\mathbb{I}_A(\mathbf{r})$ is the indicator function of the set A: $\mathbb{I}_A(\mathbf{r}) = 1$ for $\mathbf{r} \in A$, and 0 otherwise. This function can be thought of as a "counter" which is turned on whenever the diffusing species resides in A. One can estimate, for instance, the "trapping" time that particles spend in deep and almost enclosed pores (like fjords) of a catalyst.

With this technique, one can easily assess much finer and more detailed statistics of residence times. For instance, to compute the residence time of the diffusing species between two times $0 \le t_1 < t_2 \le t$, a counter should be forced to turn on only during this period. Since the evolution of the system during two other periods $(0, t_1)$ and (t_2, t) is unperturbed (no counting or interaction), Eq. (11) can be modified as

$$\mathbb{E}\{e^{iq\phi}\} = (U e^{-\Lambda t_1} e^{(iq\mathcal{B}-\Lambda)(t_2-t_1)} e^{-\Lambda(t-t_2)} \tilde{U}).$$

Three matrix exponentials represent three successive time periods of the evolution. This "matrix product rule" can be applied in general, when one studies the residence time for a sequence of time intervals: the matrices $e^{(iq\mathcal{B}-\Lambda)\delta t}$ and $e^{-\Lambda\delta t}$ represent the periods of duration δt with and without count-

ing, respectively. Moreover, one can change the region of interest (set A) between different time periods. For example, the characteristic function

$$\mathbb{E}\{e^{iq\phi}\} = (Ue^{(iq\mathcal{B}_1-\Lambda)t/2}e^{(-iq\mathcal{B}_2-\Lambda)t/2}\tilde{U})$$

describes the difference in residence times for diffusing particles spending the first half time period in a subset A_1 and the second half time period in a subset A_2 (note the minus sign in front of $iq\mathcal{B}_2$ to switch the counter into decreasing mode). This could be a direct quantitative measure of exchange processes between these two subsets (e.g., two pores of a medium).

Similar relations can be derived for the Laplace transforms. So the expectation $\mathbb{E}\{e^{-h\phi}\}$ can be interpreted as the survival probability of the reflected Brownian motion up to time t when h is the relaxation, reaction, or trapping rate inside the subset A. For instance, it can describe biological reactions which take place inside certain organelles. For several trapping subsets A_i with different relaxation rates h_i, $h\mathcal{B}$ in Eq. (8) is simply replaced by the sum $\Sigma_i h_i \mathcal{B}_i$. More generally, different "encoding mechanisms" $B_i(\mathbf{r})$ can be superimposed; for example, the magnetic field inhomogeneity in the whole sample and the bulk relaxation in a given subset.

While the matrix exponentials describe evolution, the vectors U and $\tilde{U}$ allow one to specify the initial and final states. If $\rho(\mathbf{r})$ and $\tilde{\rho}(\mathbf{r})$ are uniform, the orthogonality of the eigenfunctions implies $U_m = \tilde{U}_m = \delta_{m,0}$ [since the lowest eigenfunction $u_0(\mathbf{r})$ is uniform]. In this case, the characteristic function is determined by the first diagonal element of the evolution operator. On the other hand, if the starting point $\mathbf{r}_0$ and the arrival vicinity $\mathbf{r}_t$ are given, one takes $\rho(\mathbf{r}) = \delta(\mathbf{r}-\mathbf{r}_0)$ and $\tilde{\rho}(\mathbf{r}) = V\delta(\mathbf{r}-\mathbf{r}_t)$ to get $U_m = V^{1/2}u_m^*(\mathbf{r}_0)$ and $\tilde{U}_m = V^{1/2}u_m(\mathbf{r}_t)$. The reflected Brownian motion can also be conditioned to start and/or to arrive in two given regions.

In many situations, it is important to study the residence time on the interface, which is called the (boundary) local time:

$$\ell_t = \lim_{\varepsilon\to\infty} \frac{1}{\varepsilon}\int_0^t ds\, \mathbb{I}_{\partial\Omega_\varepsilon}(X_s), \tag{28}$$

where $\partial\Omega_\varepsilon$ is the ε vicinity of the boundary $\partial\Omega$: $\partial\Omega_\varepsilon = \{\mathbf{r}\in\Omega:\ |\mathbf{r}-\partial\Omega| \le \varepsilon\}$. The local time ℓ_t is related to the statistics of finite-distance reflections from the boundary, which is crucial for intermittent Brownian dynamics [29–32]. In addition, the local time plays an important role in the definition of partially reflected Brownian motion [41] and spread harmonic measures [42], determining the properties of the Laplacian transport toward irregular interfaces [43,44]. The characteristic function of the local time is given by Eq. (11) with the matrix $\mathcal{B}$ determined by substituting $B(\mathbf{r}) = \mathbb{I}_{\partial\Omega_\varepsilon}(\mathbf{r})/\varepsilon$ in Eq. (6). When normalized by ε, the integral over the ε vicinity $\partial\Omega_\varepsilon$ converges to the surface integral over the (smooth) boundary $\partial\Omega$, yielding

$$\mathcal{B}_{m,m'} = \int_{\partial\Omega} d\mathbf{r}\, u_m^*(\mathbf{r})u_{m'}(\mathbf{r}). \tag{29}$$

Here, the passage to the limit $\varepsilon\to 0$, which is in general delicate and time consuming for numerical techniques (see below), is implemented intrinsically. This is one of the crucial advantages of the matrix formalism for computing local times.

III. NUMERICAL IMPLEMENTATION

The present approach is a mathematical basis for efficient numerical calculation of the residence and local times. The increasing eigenvalues λ_m enable one to truncate both matrices Λ and $\mathcal{B}$ to moderate sizes, allowing rapid and very accurate computation of the matrix exponentials in Eq. (11) or similar relations. In this section, we illustrate the advantages of this technique in comparison to conventional methods like Monte Carlo simulations.

A. Matrix formalism

For simple domains like a slab, cylinder, and sphere, the Laplace operator eigenbasis is known explicitly, and the numerical computation for a given functional in Eq. (1) is straightforward. To illustrate this point, we consider the local time of reflected Brownian motion in a slab of width 1 (i.e., the unit interval). In this case, the eigenvalues and eigenfunctions of the Laplace operator are

$$\lambda_m = \pi^2 m^2, \quad u_m(x) = \epsilon_m \cos(\pi m x),$$

with the normalization constants $\epsilon_m = \sqrt{2}$ for $m>0$, and $\epsilon_0 = 1$. According to Eq. (28), the local time statistics can be determined by taking for $B(\mathbf{r})$ the normalized indicator function of an ε vicinity of the confining domain. In the case of a slab, it corresponds to two segments $(0,\ \varepsilon)$ and $(1-\varepsilon,\ 1)$ of length ε near the end points 0 and 1, respectively:

$$B^\varepsilon(x) = \frac{1}{\varepsilon}[\Theta(x) - \Theta(x-\varepsilon) + \Theta(x-1+\varepsilon) - \Theta(x-1)],$$

$\Theta(x)$ being the Heaviside step function: $\Theta(x)=1$ for $x>0$, and 0 otherwise. Direct integration in Eq. (27) yields a simple structure of the corresponding matrix $\mathcal{B}^\varepsilon$:

$$\mathcal{B}^\varepsilon_{m,m'} = \mathcal{B}_{m,m'}\left(\frac{\sin[\pi\varepsilon(m-m')]}{2\pi\varepsilon(m-m')} + \frac{\sin[\pi\varepsilon(m+m')]}{2\pi\varepsilon(m+m')}\right), \tag{30}$$

where

$$\mathcal{B}_{m,m'} = \epsilon_m\epsilon_{m'}[1+(-1)^{m-m'}]. \tag{31}$$

When ε goes to 0, the expression in large parentheses tends to 1, implying that the elements $\mathcal{B}^\varepsilon_{m,m'}$ converge to $\mathcal{B}_{m,m'}$. Substituting these elements from Eq. (30) in Eqs. (25), one obtains $b_{1,1}=2$, independently of ε, and

$$b_{2,1}^{\varepsilon} = \frac{4}{\pi^2} \sum_{m=1}^{\infty} \frac{1}{m^2} \left(\frac{\sin 2\pi\varepsilon m}{2\pi\varepsilon m} \right)^2. \tag{32}$$

In the limit $\varepsilon \to 0$, one has $b_{2,1}=2/3$. This value could alternatively be found by substituting the elements $\mathcal{B}_{m,m'}$ from Eq. (31) in Eqs. (25).

In general, the direct use of the matrix $\mathcal{B}$ instead of $\mathcal{B}^{\varepsilon}$ would not only simplify the computation but, more importantly, perform the passage to the limit $\varepsilon \to 0$. As already mentioned, this is one of the crucial computational advantages of the matrix formalism in comparison with other techniques. For instance, Monte Carlo simulations require a finite ε vicinity for computing the local times, and the computation becomes longer as ε is decreased (see below).

B. Monte Carlo simulations

To illustrate the advantage of the matrix technique, we calculate the local time statistics by using Monte Carlo simulations. For a fixed t, the time interval $[0,t]$ is divided into n subintervals of duration $\delta=t/n$. Small displacements of a Brownian particle on the interval (0,1) are modeled as independent normally distributed random jumps with variance 2δ (the diffusion coefficient is 1). The starting point is chosen randomly over the unit interval (uniform initial density). If the Brownian particle jumps beyond the end point 0 or 1, it is reflected back to the unit interval. For each simulated trajectory, the local time is approximated as a fraction of steps (normalized by ε) at which the Brownian particle stayed in either the subinterval $(0,\varepsilon)$ or $(1-\varepsilon,\ 1)$. No condition on the arrival points is imposed (uniform weight function).[4] The probability distribution of the local time is approximated by simulating N trajectories of the reflected Brownian motion. Similar Monte Carlo simulations were implemented for a disk and a sphere.

Three computational parameters have to be chosen: the width ε, the number n of subintervals, and the number N of trajectories (walkers). The explicit formula (32) can be used as a sort of criterion for the choice of a reliable value for ε. Figure 3 shows the coefficient $b_{2,1}^{\varepsilon}$ as a function of ε. One clearly sees the convergence to the limiting value 2/3 as $\varepsilon \to 0$. For a numerical simulation, the width ε should be chosen inferior to 0.01 in order to get accurate statistics of the local times. In what follows, ε is fixed to be 0.01.

For accurate modeling of the reflected Brownian motion in ε vicinities of the boundary, the typical displacement $\sqrt{2\delta}$ at each step should be much smaller than the width ε. This condition yields a restriction for the choice of the number n of subintervals: $n \gg 2t/\varepsilon^2$ (since $\delta=t/n$). In this study, we consider the time t up to 10 which requires n to be taken on the order of 10^6.

Finally, the accuracy of the results obtained by Monte Carlo simulations is of the order of $1/\sqrt{N}$. We chose $N=10^6$ to get the moments with three significant digits. It is worth noting that these moments still remain approximate since the width ε is fixed so that the limit $\varepsilon \to 0$ is not taken.

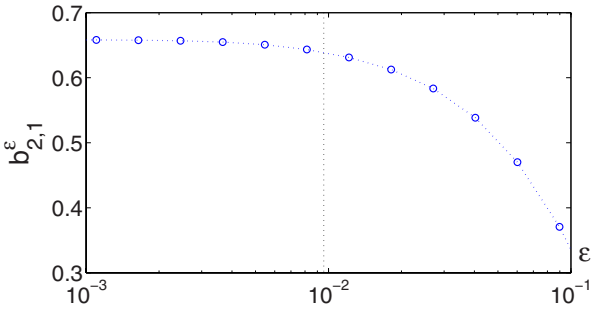

FIG. 3. (Color online) Coefficient $b_{2,1}^{\varepsilon}$ for different ε vicinities of the boundary of the unit interval.

Although each simulation step in Monte Carlo simulations is extremely simple and rapid, the large number of these steps ($nN=10^{12}$) results in long computational times. The algorithm has been implemented in C and ran on an Althon 1.4 GHz processor for around 50 h. In principle, this computational time could be reduced by code optimization or parallel computation, but it would still remain much longer than the few seconds computation via matrix formalism.

C. Numerical results

In this section, we present several numerical results, mainly for illustrative purpose. A thorough numerical study of the residence and local times of the reflected Brownian motion will be presented elsewhere.

In Table I, we compare the theoretical and numerical values of the first four cumulant moments of the local time of the reflected Brownian motion on the unit interval for uniform initial density and weight function. Their theoretical calculation is based on the explicit form of the matrix $\mathcal{B}$ for the unit interval (see Appendices). For more complex domains, for which an explicit form is not available, the infinite-dimensional matrices $\mathcal{B}$ and Λ should be truncated to moderate sizes $M \times M$ and then computed numerically. To

TABLE I. First four cumulant moments of the local time of the reflected Brownian motion on the unit interval at $t=10$ for uniform initial density and weight function. The analytic results at long time (obtained by using the coefficients from Table IV) are compared to those computed numerically by truncation of the governing matrices up to $M=100$ (third column), and by Monte Carlo simulation (fourth column). Relative errors of the numerical values are indicated in parentheses.

	Theory	Matrix approach	Monte Carlo
$<\phi>$	20.000	20.000(0.0%)	19.999(0.0%)
$<\phi^2>$	6.661	6.579(1.2%)	6.391(4.1%)
$<\phi^3>$	2.665	2.584(3.1%)	2.391(10.3%)
$<\phi^4>$	1.016	0.951(6.4%)	0.461(54.6%)

[4]It is worth noting that Monte Carlo simulations for reflected Brownian motion conditioned to arrive at time t in a small vicinity of some point $\mathbf{r}$ are much more time consuming. Indeed, only a very small fraction of trajectories arrive in this vicinity so that most simulations have to be rejected.

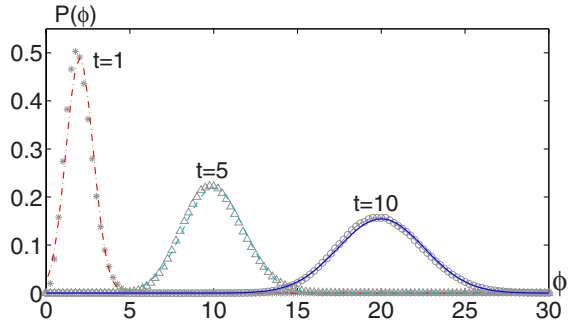

FIG. 4. (Color online) Probability distribution of the local time of reflected Brownian motion on the unit interval at times $t=1$, 5, 10 (stars, triangles, and circles, respectively), and its Gaussian approximation (26) with $b_{1,1}=2$ and $b_{2,1}=2/3$ (dashed-dotted, dashed, and solid lines, respectively).

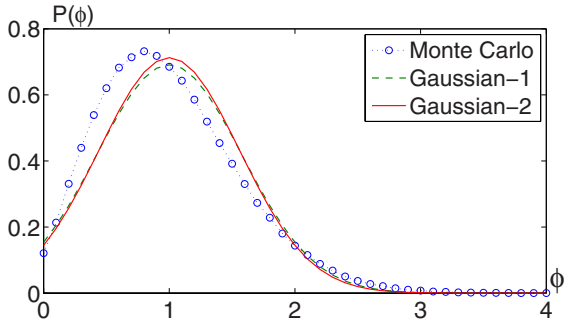

FIG. 5. (Color online) Probability distribution of the local time of reflected Brownian motion on the unit interval at time $t=0.5$ (circles), and two Gaussian approximations: the basic approximation (26) with $b_{1,1}t=1$ and $b_{2,1}t=1/3$ (dashed line); and a more accurate approximation with the same mean 1 but the variance $<\phi^2>\simeq 0.31$, accounting for finite width $\varepsilon=0.01$ (solid line).

evaluate the accuracy of this approximation in the case of the unit interval, we computed the cumulant moments by taking $M=100$ (third column in Table I). The results of Monte Carlo simulations are shown in the last column. The mean local time (the first moment) is found accurately by both numerical techniques. As expected, higher-order cumulant moments, representing finer statistical properties of the probability distribution, are found with lower accuracy. The matrix approach gives systematically better results. It is worth noting, however, that the choice of the unit interval as a confining domain allowed us to use the explicit form of the Laplace operator eigenbasis. In general, the accuracy of the matrix formalism is limited by the accuracy of numerical tools used to find this eigenbasis in a given domain. Although this computation may be time consuming for complex shapes, it has to be performed only once as a preliminary step, allowing then for a rapid calculation of any residence or local time.

More elaborate analysis of the cumulant moments by Monte Carlo simulations is difficult or even impossible. For instance, a linear fit of the cumulant moment $<\phi^n>$ as a function of time t might in principle be used to compute the coefficients $b_{n,0}$ and $b_{n,1}$. However, such a linear dependence holds only for long enough time, thus prohibiting an accurate computation of $b_{n,0}$. In contrast, the matrix formalism provides explicit separate relations for both coefficients.

As shown in Sec. II C, the probability distribution of the local time is getting closer and closer to normal as the exploration time t increases. Figure 4 illustrates this statement by comparing the Monte Carlo simulations to a Gaussian approximation (26) with $b_{1,1}=2$ and $b_{2,1}=2/3$ at times $t=1$, 5, 10. Even for $t=1$, the Gaussian approximation is a relatively accurate approximation. Similar results (not presented here) were obtained for a disk and a sphere.

To investigate the deviation from Gaussian behavior, we consider the probability distribution for a still smaller time $t=0.5$. Figure 5 shows the numerical data obtained by Monte Carlo simulations, and two Gaussian approximations. The first one is given by Eq. (26), which accounts neither for coefficient $b_{2,0}$, nor for a finite width ε. These two features are corrected in the second Gaussian approximation, with the variance $<\phi^2>$ equal to 0.31. In spite of this correction, both Gaussian approximations appear slightly on the right with respect to the numerical data. This deviation has two sources: higher-order cumulant moments give significant contributions that cannot be neglected at small t; and exponential corrections to the moments are also not negligible and should be taken into account.

The deviation from the Gaussian distribution becomes still larger at smaller time t.

It is worth noting that all probability distributions we discussed above could be derived without Monte Carlo simulations by using the matrix formalism alone. This computation (not presented here) is based on the inverse Laplace or Fourier transform of Eq. (8) or Eq. (11), respectively. We believe that the comparison between our theoretical results and those produced by a *different* computational technique (Monte Carlo simulations) is more convincing.

IV. CONCLUSION

In conclusion, we presented an efficient approach to investigate residence times and other functionals of reflected Brownian motion. In sharp contrast with previous works, focused mainly on the mean residence time or limiting distributions, the present approach allows for determination of the full probability distribution. Its Fourier transform (characteristic function) and Laplace transform (survival probability) were obtained in a compact matrix form involving the Laplace operator eigenbasis. The matrix exponentials in Eq. (11) or similar relations are easy to calculate numerically once the governing matrices $\mathcal{B}$ and Λ are constructed for a given confining geometry. The concepts developed can be extended to more complicated stochastic processes governed by a general second-order elliptic differential operator having a complete eigenbasis. One can also consider "composite" boundary conditions when one part of the interface remains reflecting (Neumann), while the other is absorbing (Dirichlet). In this case, "exit" or "stopping" events can be incorporated.

The moments of residence times have been studied. The use of the matrix representation allowed us to show that the

moment $\mathbb{E}\{\phi^n\}$ is a polynomial of degree n at long time t. The coefficients of this polynomial are expressed through the two governing matrices $\mathcal{B}$ and Λ and vectors U and $\tilde{U}$ by using a diagram representation. Moreover, any cumulant moment $<\phi^n>$ was argued to be a linear function of t. This statement was demonstrated for the cumulant moments up to the order 4 and checked numerically for several higher orders. As a consequence, the normalized residence time $\phi/\sqrt{t}$ is getting closer and closer to a Gaussian variable as time t grows. These theoretical results have been successfully confronted with Monte Carlo simulations.

ACKNOWLEDGMENTS

The author acknowledges Dr. P. Levitz and Dr. C. Boutillier for fruitful discussions. The work has been supported by the ANR Project MIPOMODIM Grant No NT05-1_42030.

APPENDIX A: MOMENTS AT LONG TIME

As discussed in Sec. II B, Eqs. (15) and (16) establish an exact but still complicated representation for the moment $\mathbb{E}\{\phi^n\}$, requiring summation of multiple coupled infinite series. Using the exact formula (16) for the function $F_n(t;\lambda_{m_1},\ldots,\lambda_{m_{n+1}})$, it is thus difficult to derive analytical results. However, when time t is long enough, many terms in Eq. (15) are exponentially small. Their omission yields the approximate but very accurate formula (18) which is repeatedly used in the remainder of these appendices. The computation of the moment $\mathbb{E}\{\phi^n\}$ at long time t is then reduced to various choices of the indices $m_1,\ldots,m_{n+1}$ leading to nontrivial contributions to Eq. (15).

Using the explicit form (18), one can derive many properties of the function $F_n(t;\lambda_{m_1},\ldots,\lambda_{m_{n+1}})$. So, when j among $n+1$ of its arguments are zero, this function is a polynomial of degree $j-1$. For instance,

$$F_n(t;\underbrace{0,\ldots,0}_{i-1},\lambda_m,\underbrace{0,\ldots,0}_{n+1-i}) \simeq \frac{(-1)^{n-1}}{\lambda_{m_i}^n}\sum_{k=0}^{n-1}\frac{(-t\lambda_{m_i})^k}{k!} \tag{A1}$$

for $j=n$ [the result is independent of the position i of the nonzero entry λ_{m_i} among the other (zero) entries]. In general, the moment $\mathbb{E}\{\phi^n\}$ as a function of time t turns out to be a polynomial of degree n. In what follows, we investigate the coefficients $a_{n,k}$ of this polynomial, defined as in Eq. (19).

As discussed in Sec. II C, the coefficient $a_{n,n}$ in front of the highest-degree term t^n is determined by Eqs. (15) and (17) when all $n+1$ indices $m_1,\ldots,m_{n+1}$ are equal to 0. According to Eq. (A1), the next term t^{n-1} is provided by such combinations of indices $m_1,\ldots,m_{n+1}$ that n of them are zero. Collecting all these combinations, one finds the coefficient in front of t^{n-1}:

$$\begin{aligned} a_{n,n-1} = n\sum_{m=1}^{\infty}\,&(U_m\lambda_m^{-1}\mathcal{B}_{m,0}\mathcal{B}_{0,0}\cdots\mathcal{B}_{0,0}\tilde{U}_0 \\ &+ U_0\mathcal{B}_{0,m}\lambda_m^{-1}\mathcal{B}_{m,0}\mathcal{B}_{0,0}\cdots\mathcal{B}_{0,0}\tilde{U}_0+\cdots \\ &+ U_0\mathcal{B}_{0,0}\mathcal{B}_{0,0}\cdots\mathcal{B}_{0,m}\lambda_m^{-1}\tilde{U}_m), \end{aligned} \tag{A2}$$

the ith term corresponding to the choice of the nonzero index m_i. In spite of the simplicity of this relation, it is convenient to give another representation in matrix form. For this purpose, we introduce two infinite-dimensional matrices:

$$\mathcal{A}_{m,m'} = \begin{cases} \delta_{m,m'}\lambda_m^{-1}, & m>0 \text{ and } m'>0, \\ 0, & m=0 \text{ or } m'=0, \end{cases}$$

$$\mathcal{O}_{m,m'} = \delta_{m,0}\delta_{m',0}. \tag{A3}$$

The first matrix $\mathcal{A}$ will be used to represent the summation over the inverse eigenvalues λ_m^{-1}, taking also into account that the summation should start with $m=1$ (no term with $m=0$). The second matrix $\mathcal{O}$ is intended to set the summation index to 0. In fact, the matrix $\mathcal{O}$ entering between any two matrices X and Y splits them into two separate factors: $[X\mathcal{O}Y]_{m,m'}=X_{m,0}Y_{0,m'}$. Using the matrices $\mathcal{A}$ and $\mathcal{O}$, Eq. (A2) can be written in a compact matrix form

$$\begin{aligned} a_{n,n-1} = n[U\mathcal{A}\underbrace{\mathcal{B}\mathcal{O}\mathcal{B}\mathcal{O}\cdots}_{n\text{ times}}\tilde{U} + U\mathcal{O}\mathcal{B}\mathcal{A}\underbrace{\mathcal{B}\mathcal{O}\mathcal{B}\mathcal{O}\cdots}_{n-1\text{ times}}\tilde{U} + \cdots \\ + U\mathcal{O}\underbrace{\mathcal{B}\mathcal{O}\mathcal{B}\mathcal{O}\cdots}_{n-1\text{ times}}\mathcal{B}\mathcal{A}\tilde{U}]. \end{aligned} \tag{A4}$$

The above relation states that the coefficient $a_{n,n-1}$ can be obtained by considering a sequence of n matrices $\mathcal{B}$ (started and terminated by vectors U and $\tilde{U}$, respectively), putting between them n matrices $\mathcal{O}$ and one matrix $\mathcal{A}$ in all possible ways ($n+1$ terms). For further analysis, it is convenient to introduce a formal diagrammatic representation for such matrix products with the following notations: open circles, placed only once on the left (vector U) and on the right (vector $\tilde{U}$); full circle (matrix $\mathcal{B}$); solid line between circles (matrix $\mathcal{A}$); integer powers of the matrix $\mathcal{A}$ are represented by double, triple, etc., lines (see below); empty space between circles (matrix $\mathcal{O}$).

In this diagrammatic representation, the coefficient $a_{n,n-1}$ is obtained by taking a sequence of n full circles in a line (started and terminated by two open circles) and connecting two neighboring circles by one link in all possible ways:

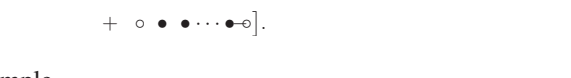

For example,

(A5)

Since the matrix $\mathcal{O}$ splits matrix products into separate parts, each of the above diagrams is a product of separate blocks, e.g.,

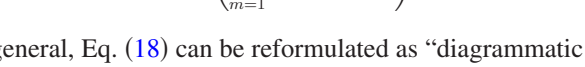

In general, Eq. (18) can be reformulated as "diagrammatic rules" for computing all coefficients $a_{n,k}$ of the polynomial (19). Tedious but still elementary combinatorial analysis

shows that $a_{n,k}$ is equal to $n!/k!$ multiplied by the sum over all diagrams formed by n full circles (preceded and succeeded by an open circle) with totally $n-k$ links. Note that double, triple, etc., links (denoting powers of $\mathcal{A}$) are allowed. Diagrams provide positive (negative) contributions to the sum when $k+k_e+1$ is even (odd), k_e being the number of empty spaces between circles (number of matrices $\mathcal{O}$). More formally, if j_i denotes the number of links between the ith and $(i+1)$th circles such that $j_1+\cdots+j_{n+1}=n-k$, then k_e is the number of such links j_i that are equal to 0, and

$$a_{n,k} = \frac{n!}{k!} \sum_{\substack{j_i \geq 0 \ \forall i \\ j_1+\ldots+j_{n+1}=n-k}} (-1)^{k+k_e+1} \ \underset{j_1}{\circ\!\sim\!\bullet} \underset{j_2}{\sim\!\bullet} \ \ldots \ \underset{j_{n+1}}{\bullet\!\sim\!\circ} \ , \tag{A6}$$

where the tilde at the ith position may denote empty space ($j_i=0$) or single, double, triple, etc., lines ($j_i=1,\ 2,\ 3,\ \ldots$). For instance, one has

$$a_{2,0} = 2\big[\circ\!-\!\bullet\!-\!\bullet\ \circ\ +\ \circ\!-\!\bullet\ \bullet\!-\!\circ\ +\ \circ\ \bullet\!-\!\bullet\!-\!\circ$$
$$-\ \circ\!=\!\bullet\ \bullet\ \circ\ -\ \circ\ \bullet\!=\!\bullet\ \circ\ -\ \circ\ \bullet\ \bullet\!=\!\circ\big]. \tag{A7}$$

APPENDIX B: CUMULANT MOMENTS

Although the moments $\mathbb{E}\{\phi^n\}$ can be found with the help of Eqs. (19) and (A6), the number of diagrams contributing to the coefficient $a_{n,k}$ grows rapidly with n. Moreover, these coefficients have to be computed for each value of k ranging from 0 to n. The computation of the moments $\mathbb{E}\{\phi^n\}$ thus becomes too lengthy even for relatively small n. The analysis can be significantly simplified by considering instead of $\mathbb{E}\{\phi^n\}$ the cumulant moments $\prec\phi^n\succ$ defined as coefficients in a series expansion (21) of the logarithm of the characteristic function. The cumulant moment $\prec\phi^n\succ$ is related through the recursion formula (23) to the moments $\mathbb{E}\{\phi^k\}$ with $1\leq k\leq n$, and vice versa [see Eq. (22) for a few examples]. As a consequence, knowledge of the cumulant moments is completely equivalent to that of the (ordinary) moments. However, a diagrammatic representation for the cumulants is in general simpler. Such a simplification comes from the fact that the cumulant moment $\prec\phi^n\succ$ captures the features of the probability distribution *precisely* at the order n, while lower-order features are explicitly subtracted so that many diagrams cancel each other. To illustrate this point, we calculate the second cumulant moment using the explicit diagrammatic representation (A5) for the coefficient $a_{2,1}$, as well as $a_{2,2}=\circ\bullet\bullet\circ$:

$$\prec\phi^2\succ = 2\big[\circ\ \bullet\!-\!\bullet\ \circ\big]t + \big[a_{2,0}-a_{1,0}^2\big].$$

In contrast with the second moment $\mathbb{E}\{\phi^2\}$, the cumulant $\prec\phi^2\succ$ is a linear function of t. The isolated diagrams $\circ$ on the left and on the right represent, respectively, U_0 and $\tilde{U}_0$, which are both equal to 1 since the lowest eigenfunction $u_0(\mathbf{r})$ is constant. One then finds the even simpler form

$$\prec\phi^2\succ = 2!\big[\bullet\!-\!\bullet\big]t + \big[a_{2,0}-a_{1,0}^2\big].$$

Although more tedious, the computation for the third and fourth cumulant moments is similar, yielding again linear dependences on t:

$$\prec\phi^3\succ = 3!\big[\bullet\!-\!\bullet\!-\!\bullet\ -\ \bullet\!=\!\bullet\ \bullet\big]t + \big[a_{3,0}-3a_{2,0}a_{1,0}+2a_{1,0}^3\big],$$
$$\prec\phi^4\succ = 4!\big[\bullet\!-\!\bullet\!-\!\bullet\!-\!\bullet\ -\ \bullet\!=\!\bullet\!-\!\bullet\ \bullet\ -\ \bullet\!-\!\bullet\!=\!\bullet\ \bullet$$
$$-\ \bullet\!=\!\bullet\ \bullet\!-\!\bullet\ +\ \bullet\!\equiv\!\bullet\ \bullet\ \bullet\big]t$$
$$+\big[a_{4,0}-4a_{3,0}a_{1,0}-3a_{2,0}^2+12a_{2,0}a_{1,0}^2-6a_{1,0}^4\big].$$

For the general case (any order n), we conjecture the following result.

(1) The zero-order coefficient $b_{n,0}$ is expressed through $a_{k,0}$, $1\leq k\leq n$, by setting $t=0$ in the recursion formula (23) for the cumulants:

$$b_{n,0} = a_{n,0} - \sum_{k=1}^{n-1} C_{n-1}^{k-1} b_{k,0} a_{n-k,0}. \tag{B1}$$

This statement does not need a proof.

(2) The first-order coefficients $b_{n,1}$ are expressed through the diagrams with disconnected open circles obtained by the following combinatorial rule. We consider n full circles in a line and connect them with $n-1$ links in all possible ways. The coefficient $b_{n,1}$ is equal to $n!$ multiplied by the sum over all *topologically different* diagrams, each of them being taken with positive (negative) sign according to the even (odd) number k_e of empty spaces. For instance, one has

$$b_{1,1} = 1!\big[\circ\ (\bullet)\ \circ\big]$$
$$b_{2,1} = 2!\big[\circ\ (\bullet\!-\!\bullet)\ \circ\big]$$
$$b_{3,1} = 3!\big[\circ\ (\bullet\!-\!\bullet\!-\!\bullet\ -\ \bullet\!=\!\bullet\ \bullet)\ \circ\big]$$
$$b_{4,1} = 4!\big[\circ\ (\bullet\!-\!\bullet\!-\!\bullet\!-\!\bullet\ -\ \bullet\!=\!\bullet\!-\!\bullet\ \bullet\ -\ \bullet\!-\!\bullet\!=\!\bullet\ \bullet$$
$$-\ \bullet\!=\!\bullet\ \bullet\!-\!\bullet\ +\ \bullet\!\equiv\!\bullet\ \bullet\ \bullet)\ \circ\big]$$

Note that the diagrams $\bullet=\bullet\!\longrightarrow\!\bullet\bullet$ and $\bullet\!\longrightarrow\!\bullet=\bullet\bullet$ are topologically different (although their numerical values are the same; see Table III), while the diagrams $\bullet=\bullet\!\longrightarrow\!\bullet\bullet$ and $\bullet\bullet=\bullet\!\longrightarrow\!\bullet$ are identical (and only one copy of them is taken into account). As previously, the isolated diagrams $\circ$ are equal to 1 and can thus be omitted.

(3) The higher-order coefficients $b_{n,k}$ with $k\geq 2$ are equal to 0.

These statements have been demonstrated above by direct calculation of the cumulant moments up to $n=4$, and checked by numerical simulations for several higher orders. A rigorous mathematical proof for any n is still missing.

APPENDIX C: LOCAL TIME FOR A SLAB

In this section, we illustrate the computation of diagrams for the local time of the reflected Brownian motion in a slab (the unit interval). We recall that the specific form of the matrix $\mathcal{O}$ relates the contribution of any diagram to the prod-

TABLE II. Exact values of the coefficients $\zeta_d(j)$ with $j=1, 2, 3, 4$ for the local time of the reflected Brownian motion in a slab ($d=1$), a disk ($d=2$), and a sphere ($d=3$).

j	1	2	3	4
$\zeta_1(j)$	1/24	1/1440	1/60480	1/2419200
$\zeta_2(j)$	1/8	1/192	1/3072	1/46080
$\zeta_3(j)$	1/10	1/350	1/7875	37/6063750

uct of contributions from its constituent *connected* diagrams, e.g., $(\bullet\!\!-\!\!\bullet\ \bullet)=(\bullet\!\!-\!\!\bullet)(\bullet)$. It is thus sufficient to compute only connected diagrams. In the case of a slab, the explicit form of the matrices $\mathcal{B}$ and Λ for the local time allows one to calculate the exact contribution of any connected diagram.

We start with the diagram $\bullet\!\!-\!\!\bullet$ which represents the first diagonal element of the matrix $\mathcal{BAB}$:

$$\bullet\!\!-\!\!\bullet = [\mathcal{BAB}]_{0,0} = \sum_{m=1}^{\infty} \mathcal{B}_{0,m}\lambda_m^{-1}\mathcal{B}_{m,0}.$$

Since $\mathcal{B}_{0,m}=\mathcal{B}_{m,0}=\sqrt{2}[1+(-1)^m]$ for $m>0$, the summation is carried out over even indices:

$$\bullet\!\!-\!\!\bullet = \sum_{m=1}^{\infty} 2\sqrt{2}\,\frac{1}{\pi^2(2m)^2}\,2\sqrt{2} = \frac{2}{\pi^2}\zeta(2),$$

where $\zeta(z)$ is the Riemann zeta function,

$$\zeta(z) = \sum_{m=1}^{\infty} \frac{1}{m^z}.$$

For a connected diagram composed of $n+1$ full circles and n links $j_1,\ldots,j_n$, one finds

$$\underset{j_1}{\bullet}\!\sim\!\underset{j_2}{\bullet}\!\sim\!\bullet\ \ldots\ \bullet\!\sim\!\underset{j_n}{\bullet} = 2^{2n+1}\prod_{k=1}^{n}\zeta_1(j_k), \tag{C1}$$

where

$$\zeta_1(j) = \frac{\zeta(2j)}{(2\pi)^{2j}}. \tag{C2}$$

Each connected diagram is then expressed in terms of the values of the Riemann ζ function at even integers. All these values are related to Bernoulli numbers B_{2k},

$$\zeta(2j) = \frac{(-1)^{j-1}(2\pi)^{2j}}{2(2j)!}B_{2j},$$

for which the generating function is known:

$$\frac{x}{e^x-1} = \sum_{k=0}^{\infty} B_k\frac{x^k}{k!}.$$

One can thus compute $\zeta_1(j)$ for any positive integer j (the first four values are given in Table II), so that any connected diagram can be found. Table III shows the values of several connected diagrams that we need to calculate the first four cumulant moments (see below).

TABLE III. Connected diagrams needed to calculate the first four cumulant moments, and their values for the local time of the reflected Brownian motion on the unit interval, disk, and sphere (with uniform initial density and weight function).

	Slab	Disk	Sphere
$\circ$	1	1	1
$\bullet$	2	2	3
$\bullet\!\!-\!\!\bullet$	1/3	1/2	3/5
$\bullet=\bullet$	1/180	1/48	3/175
$\bullet\equiv\bullet$	1/7560	1/768	2/2625
$\bullet\overset{=}{\equiv}\bullet$	1/302400	1/11520	37/1010625
$\bullet\!\!-\!\!\bullet\!\!-\!\!\bullet$	1/18	1/8	3/25
$\bullet=\bullet\!\!-\!\!\bullet$	1/1080	1/192	3/875
$\bullet\!\!-\!\!\bullet=\bullet$	1/1080	1/192	3/875
$\bullet=\bullet=\bullet$	1/64800	1/4608	3/30625
$\bullet\equiv\bullet\!\!-\!\!\bullet$	1/45360	1/3072	2/13125
$\bullet\!\!-\!\!\bullet\equiv\bullet$	1/45360	1/3072	2/13125
$\bullet\!\!-\!\!\bullet\!\!-\!\!\bullet\!\!-\!\!\bullet$	1/108	1/32	3/125
$\bullet=\bullet\!\!-\!\!\bullet\!\!-\!\!\bullet$	1/6480	1/768	3/4375
$\bullet\!\!-\!\!\bullet=\bullet\!\!-\!\!\bullet$	1/6480	1/768	3/4375
$\bullet\!\!-\!\!\bullet\!\!-\!\!\bullet=\bullet$	1/6480	1/768	3/4375

The connected diagrams with open circles can in principle be found in a similar way, although their computation depends on the initial density and weight function. If both these densities are uniform, any connected diagram containing an open circle is equal to 0. This is a simple consequence of the facts that $U_m=\tilde{U}_m=\delta_{m,0}$ and $\mathcal{A}_{m,0}=\mathcal{A}_{0,m}=0$ so that any matrix containing $U\mathcal{A}$ or $\mathcal{A}\tilde{U}$ vanishes. When the initial density and/or the weight function is not uniform, the computation can be performed in a similar way. If the odd components of the vectors U and $\tilde{U}$ are equal to 0, one finds for a connected diagram composed of $n+1$ full circles and two open circles with $(n+2)$ links $j_0,j_1,\ldots,j_n,j_{n+1}$ (given that $j_0>0$ and $j_{n+1}>0$):

$$\underset{j_0}{\circ}\!\sim\!\underset{j_1}{\bullet}\!\sim\!\bullet\ \ldots\ \bullet\!\sim\!\bullet\!\sim\!\underset{j_{n+1}}{\circ} = \underset{j_1}{\bullet}\!\sim\!\bullet\ \ldots\ \bullet\!\sim\!\underset{j_n}{\bullet} \times\left(\sqrt{2}\sum_{m=1}^{\infty}\frac{U_{2m}}{\lambda_{2m}^{j_0}}\right)\left(\sqrt{2}\sum_{m=1}^{\infty}\frac{\tilde{U}_{2m}}{\lambda_{2m}^{j_{n+1}}}\right). \tag{C3}$$

The first factor in the right-hand side is given by Eq. (C1), while the last two factors can be written in a matrix form as $U\mathcal{AE}$ and $\mathcal{EA}\tilde{U}$, where the new vector $\mathcal{E}$ reduces the summation to even indices, $\mathcal{E}_m=[1+(-1)^m]/\sqrt{2}$. In general, a second contribution appears from summation over odd indices.

Using these results, one can analytically calculate any cumulant moment of the local time of the reflected Brownian motion in a slab at long time. So, in the case of uniform initial density and weight function, the coefficients $b_{n,k}$ determining the first four cumulant moments are given in Table IV.

TABLE IV. Coefficients $b_{n,k}$ determining the first four cumulant moments for the local time of the reflected Brownian motion on the unit interval, disk, and sphere (with uniform initial density and weight function).

	Slab	Disk	Sphere
$b_{1,1}$	2	2	3
$b_{2,1}$	2/3	1	6/5
$b_{3,1}$	4/15	1/2	72/175
$b_{4,1}$	32/315	1/8	0
$b_{1,0}$	0	0	0
$b_{2,0}$	−1/90	−1/24	−6/175
$b_{3,0}$	−1/126	−1/32	−12/875
$b_{4,0}$	−73/18900	1/960	3492/336875

APPENDIX D: DISK AND SPHERE

The computation of the diagrams for the local time of the reflected Brownian motion in a disk (cylinder) and a sphere is very similar.

1. Disk

For a disk (or an infinite cylinder) of unit radius, the classical representation of the eigenfunctions involves two positive indices n and k [34,46–48],

$$u_{nk}(r,\varphi) = \frac{\varepsilon_n}{\sqrt{\pi}} \frac{\beta_{nk}}{J_n(\alpha_{nk})} J_n(\alpha_{nk} r)\cos(n\varphi),$$

where $J_n(z)$ are the Bessel functions of the first kind. The eigenvalues $\lambda_{nk}=\alpha_{nk}^2$ are expressed through the positive zeros α_{nk} of the functions $J_n'(z)$, and the normalization constants β_{nk} are

$$\beta_{nk} = \left(\frac{\lambda_{nk}}{\lambda_{nk} - n^2} \right)^{1/2}.$$

Substitution of these eigenfunctions in Eq. (29) yields

$$\mathcal{B}_{nk,n'k'} = 2\delta_{n,n'} \beta_{nk} \beta_{nk'}. \tag{D1}$$

2. Sphere

For a sphere of unit radius, the eigenfunctions are

$$u_{nk}(r,\theta) = \frac{1}{\sqrt{2\pi}} \frac{\beta_{nk}}{j_n(\alpha_{nk})} j_n(\alpha_{nk} r) P_n(\cos\,\theta),$$

where the third index and the polar coordinate are omitted [34,46–48]. Here $P_n(x)$ are the Legendre polynomials, and $j_\nu(z)=(\pi/2z)^{1/2} J_{\nu+1/2}(z)$ the spherical Bessel functions. The eigenvalues $\lambda_{nk}=\alpha_{nk}^2$ are expressed through the positive zeros of the functions $j_n'(z)$, and the normalization constants β_{nk} are

$$\beta_{nk} = \left(\frac{(2n+1)\lambda_{nk}}{\lambda_{nk} - n(n+1)} \right)^{1/2},$$

and $\beta_{00}=\sqrt{3/2}$. Substitution of these eigenfunctions in Eq. (29) yields

$$\mathcal{B}_{nk,n'k'} = 2\delta_{n,n'} \frac{\beta_{nk}\beta_{nk'}}{2n+1}. \tag{D2}$$

3. Connected diagrams

Assuming again a uniform initial density and weight function, we focus on the computation of the connected diagrams without open circles. The specific structure of the matrix $\mathcal{B}$ allows for calculation of the exact analytical values for any connected diagram of this kind, having $(n+1)$ full circles in a line and n links $j_1,\ldots,j_n$:

$$\underset{j_1}{\bullet}\!\sim\!\underset{j_2}{\bullet}\!\sim\!\bullet \;\ldots\; \bullet\!\sim\!\underset{j_n}{\bullet} = 2^n d \prod_{k=1}^{n} \zeta_d(j_k), \tag{D3}$$

where

$$\zeta_d(j) = \sum_{k=1}^{\infty} \lambda_{0k}^{-j}, \tag{D4}$$

with the sum over the Laplace operator eigenvalues λ_{0k} either for a disk $(d=2)$ or for a sphere $(d=3)$.

To calculate the values of these sums for integer j, we introduce their generating function as

$$\tilde{\eta}_d(s) \equiv \sum_{k=1}^{\infty} \frac{1}{s+\lambda_{0k}}. \tag{D5}$$

Since $\lambda_{0k}=\alpha_{0k}^2$ and α_{0k} are zeros of some explicit functions, the generating function can be found analytically as explained in [34,46]:

$$\tilde{\eta}_1(s) = \frac{\cosh\sqrt{s}}{2\sqrt{s}\,\sinh\sqrt{s}} - \frac{1}{2s},$$

$$\tilde{\eta}_2(s) = \frac{iJ_0(i\sqrt{s})}{2\sqrt{s}J_1(i\sqrt{s})} - \frac{1}{s},$$

$$\tilde{\eta}_3(s) = \frac{\sinh\sqrt{s}}{2(\sqrt{s}\,\cosh\sqrt{s} - \sinh\sqrt{s})} - \frac{3}{2s}$$

[the first formula is applicable for direct computation of $\zeta_1(j)$ for a slab]. Their multiple differentiations yield

$$\zeta_d(j) = \frac{(-1)^{j-1}}{(j-1)!} \left(\frac{\partial^{j-1} \tilde{\eta}_d(s)}{\partial s^{j-1}} \right)_{s=0}. \tag{D6}$$

The values for $j=1,\ 2,\ 3,\ 4$ are shown in Table II, while Tables III and IV contain the connected diagrams and coefficients $b_{n,0}$ and $b_{n,1}$, respectively.

[1] G. H. Weiss, *Aspects and Applications of the Random Walk* (North-Holland, Amsterdam, 1994).
[2] S. Redner, *A Guide to First-Passage Processes* (Cambridge University Press, Cambridge, England, 2001).
[3] K. Allinger and A. Blumen, J. Chem. Phys. **75**, 2762 (1981).
[4] A. Blumen and G. Zumofen, J. Chem. Phys. **75**, 892 (1981); **76**, 3713 (1982).
[5] A. Szabo, J. Phys. Chem. **93**, 6929 (1989).
[6] A. H. Gandjbakhche and G. H. Weiss, Phys. Rev. E **61**, 6958 (2000).
[7] M. Kac, Trans. Am. Math. Soc. **65**, 1 (1949).
[8] M. Kac, in *Proceedings of the Second Berkeley Symposium on Mathematical and Statistical Problems*, edited by J. Neyman (University of California Press, Berkeley, 1951), pp. 189–215.
[9] D. A. Darling and M. Kac, Trans. Am. Math. Soc. **84**, 444 (1957).
[10] N. Agmon, J. Chem. Phys. **81**, 3644 (1984).
[11] A. M. Berezhkovskii, V. Zaloj, and N. Agmon, Phys. Rev. E **57**, 3937 (1998).
[12] A. Dhar and S. N. Majumdar, Phys. Rev. E **59**, 6413 (1999).
[13] L. Dagdug, A. M. Berezhkovskii, and G. H. Weiss, Phys. Rev. E **66**, 012901 (2002).
[14] S. Blanco and R. Fournier, Europhys. Lett. **61**, 168 (2003).
[15] A. Mazzolo, Europhys. Lett. **68**, 350 (2004).
[16] J. D. Noh and H. Rieger, Phys. Rev. Lett. **92**, 118701 (2004).
[17] O. Benichou, M. Coppey, J. Klafter, M. Moreau, and G. Oshanin, J. Phys. A **38**, 7205 (2005).
[18] S. Majumdar, Curr. Sci. **89**, 2076 (2005).
[19] E. Barkai, J. Stat. Phys. **123**, 883 (2006).
[20] K. R. Brownstein and C. E. Tarr, Phys. Rev. A **19**(6), 2446 (1979).
[21] P. T. Callaghan, *Principles of Nuclear Magnetic Resonance Microscopy* (Clarendon, Oxford, 1991).
[22] G. F. Froment and K. B. Bischoff, *Chemical Reactor Analysis and Design* (John Wiley & Sons, New York, 1990).
[23] J. M. Thomas and W. J. Thomas, *Principles and Practice of Heterogeneous Chemistry* (VCH, Weinheim, 1997).
[24] B. Sapoval, in *Fractals and Disordered Systems*, edited by A. Bunde and S. Havlin (Springer, Berlin, 1996), pp. 233–261.
[25] E. R. Weibel, *The Pathway for Oxygen. Structure and Function in the Mammalian Respiratory System* (Harvard University Press, Cambridge, MA, 1984).
[26] M. Felici, M. Filoche, C. Straus, T. Similowski, and B. Sapoval, Respir. Physiol. Neurobiol. **145**, 279 (2005).
[27] S. Condamin, O. Bénichou, and M. Moreau, Phys. Rev. Lett. **95**, 260601 (2005); Phys. Rev. E **72**, 016127 (2005); **75**, 021111 (2007).
[28] O. Bénichou, M. Coppey, M. Moreau, P. H. Suet, and R. Voituriez, Europhys. Lett. **70**, 42 (2005).
[29] O. V. Bychuk and B. O'Shaughnessy, Phys. Rev. Lett. **74**, 1795 (1995).
[30] S. Stapf, R. Kimmich, and R.-O. Seitter, Phys. Rev. Lett. **75**, 2855 (1995).
[31] P. E. Levitz, J. Phys.: Condens. Matter **17**, S4059 (2005).
[32] P. Levitz, D. S. Grebenkov, M. Zinsmeister, K. Kolwankar, and B. Sapoval, Phys. Rev. Lett. **96**, 180601 (2006).
[33] M. Freidlin, *Functional Integration and Partial Differential Equations* (Princeton University Press, Princeton, NJ, 1985).
[34] D. S. Grebenkov, Rev. Mod. Phys. **79**, 1077 (2007).
[35] H. C. Torrey, Phys. Rev. **104**, 563 (1956).
[36] A. Caprihan, L. Z. Wang, and E. Fukushima, J. Magn. Reson., Ser. A **118**, 94 (1996).
[37] P. T. Callaghan, J. Magn. Reson. **129**, 74 (1997).
[38] A. V. Barzykin, Phys. Rev. B **58**, 14171 (1998); J. Magn. Reson. **139**, 342 (1999).
[39] S. Axelrod and P. N. Sen, J. Chem. Phys. **114**, 6878 (2001).
[40] H. Wilf, *Generating Functionology*, 2nd ed. (Academic, New York, 1993).
[41] D. S. Grebenkov, in *Focus on Probability Theory*, edited by L. R. Velle (Nova Science Publishers, New York, 2006), pp. 135–169.
[42] D. S. Grebenkov, Fractals **14**, 231 (2006).
[43] B. Sapoval, Phys. Rev. Lett. **73**, 3314 (1994).
[44] D. S. Grebenkov, M. Filoche, and B. Sapoval, Phys. Rev. E **73**, 021103 (2006).
[45] D. S. Grebenkov, J. Chem. Phys. **126**, 104706 (2007).
[46] D. S. Grebenkov, Diff. Fundam. **5**, 1 (2007).
[47] H. S. Carslaw and J. C. Jaeger, *Conduction of Heat in Solids*, 2nd ed. (Clarendon, Oxford, 1959).
[48] J. Crank, *The Mathematics of Diffusion*, 2nd ed. (Clarendon, Oxford, 1975).